applied sciences

MDPI

Article

High-Performance Flux Tracking Controller for Reluctance Actuator

Yang Liu, Qian Miao and Yue Dong *

Center of Ultra-Precision Optoelectronic Instrument Engineering, Harbin Institute of Technology, Harbin 150080, China; lghit@126.com (Y.L.); qmiaohit@163.com (Q.M.)
* Correspondence: ydonghit@hit.edu.cn

Abstract: To meet the ever-increasing demand for next-generation lithography machines, the actuator plays an important role in the achievement of high acceleration of the wafer stage. However, the voice coil motor, which is widely used in high-precision positioning systems, is reaching its physical limits. To tackle this problem, a novel way to design the actuator using the magnetoresistance effect is argued due to the high force densities. However, the strong nonlinearity limits its application in the nan-positioning system. In particular, the hysteresis is coupled with eddy effects and displacement, which lead to a rate-dependent and displacement-dependent hysteresis effect in the reluctance actuator. In this paper, a Hammerstein structure is used to model the rate-dependent reluctance actuator. At the same time, the displacement-dependent of the model is regarded as the interference with the system. Additionally, a control strategy combining inverse model compensation and the disturbance observer-based discrete sliding mode control was proposed, which can effectively suppress the hysteresis effect. It is worthy pointing out that the nonlinear system is transformed into a linear system with inversion bias and disturbance by the inverse model compensation. What is more, the sliding mode controller based on the disturbance observer is designed to deal with the unmodeled dynamics, displacement disturbances, and model identification errors in linear systems. Thus, the tracking performance and robustness to external disturbances of the system are improved. The simulation results show that it is superior to the PI controller combined with an inverse compensator and even to the discrete sliding mode controller connected with inverse compensator, confirming the effectiveness of the novel control method in alleviating hysteresis.

Keywords: reluctance actuator; Hammerstein structure; hysteresis; disturbance observer; discrete sliding mode control

check for updates

Citation: Liu, Y.; Miao, Q.; Dong, Y. High-Performance Flux Tracking Controller for Reluctance Actuator. *Appl. Sci.* **2023**, *13*, 10811. https://doi.org/10.3390/app131910811

Academic Editor: Gang Lei

Received: 2 August 2023
Revised: 4 September 2023
Accepted: 23 September 2023
Published: 28 September 2023

Copyright: © 2023 by the authors. Licensee MDPI, Basel, Switzerland. This article is an open access article distributed under the terms and conditions of the Creative Commons Attribution (CC BY) license (https://creativecommons.org/licenses/by/4.0/).

1. Introduction

The wafer stage and reticle stage, shown in Figure 1, are important units used in the lithography machine. In practice, the desired IC pattern is optically transferred onto a silicon wafer via a reticle mask that contains a slit for exposing light on the wafer. Since one wafer can have many ICs, the wafer needs to be repositioned from exposure to exposure. The exposure itself takes place during a scanning motion of the wafer and the reticle [1,2].

As shown in Figure 2, the reticle stage and wafer stage consist of a long-stroke stage and a short-stroke stage [3,4], in which the long stroke achieves the large stroke and coarse positioning. Meanwhile, the short-stroke stage is responsible for fine positioning accuracy. The voice coil motor is widely used in high-precision positioning systems due to the high linearity argued in [5,6].

However, with the increasing demand for throughput, the reticle and wafer stages must be operated at higher speeds and accelerations. Voice coil motors (VCM), however, are near their physical limit and cannot provide large enough thrust for the required high acceleration in the photolithography. Thus, a novel reluctance actuator is proposed in [7–9]. Compared with VCM, the reluctance motor has the advantages of high output density and

low energy consumption, but the strong hysteresis nonlinearity restricts the control accuracy of the reluctance actuator and limits its application in the high-precision positioning system [10–13], especially when hysteresis is coupled with the displacement effect and eddy current effect, which lead to displacement-dependent and rate-dependent hysteresis in the reluctance actuator. For this reason, pursuing a way of alleviating displacement-dependent and rate-dependent hysteresis in the reluctance actuator is crucial in the high precision control of the reluctance actuator.

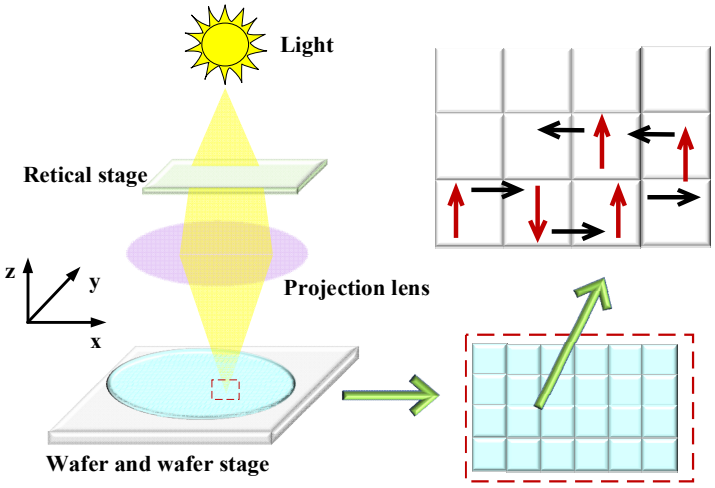

Figure 1. Diagram of a lithography scanner.

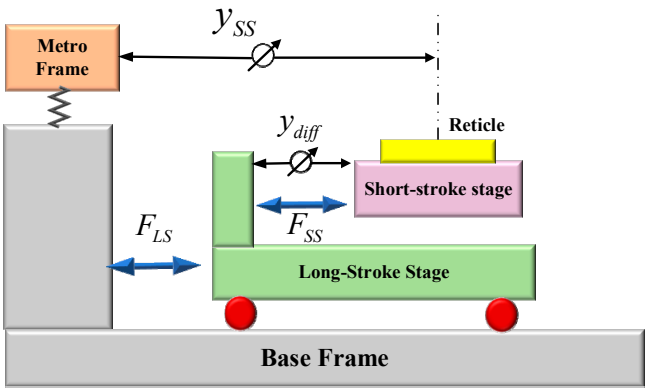

Figure 2. 1-DoF model of reticle stage.

According to the survey, one of the most general ways to suppress hysteresis is with flux feedback in a reluctance actuator. For example, in [10], the Hall element is used to measure the flux signal in the air gap, then the signal is used as a feedback variable. Whereas the method which uses the Hall element to measure flux signal in [10] sacrifices the travel of the reluctance actuator, which limits the application in the minimum air gap, thus reducing the motor efficiency. In order to tackle this problem and improve the efficiency of the reluctance motor, in [11], a sense coil sensor was used to measure the flux signal, and a shear hysteresis model, which considers the effect of displacement on the hysteresis loop, was proposed. However, the model is complex, which makes the controller design very difficult, so its application is limited. Thus, up to now, the reluctance actuator has not been adequately investigated, which gives rise to the motivation of our research.

It is worth pointing out that the control methods of hysteresis nonlinearity, which alleviates the rate-dependent hysteresis, are affluent in the Piezoelectric actuator. For example, feedforward control [14–17], namely inverse model compensation control, was widely used. In application, the inverse of the hysteresis is obtained first; then, to utilize the inverse hysteresis as the input of the system was proposed to eliminate the hysteresis

effect as well as feedback control methods, which include the PI controller [18], adaptive control method [19], sliding mode controller, and so on [20,21]. Specifically, according to the hysteresis model, the nonlinear feedback controller is designed directly, which drives the object to keep consistent with the desired trajectory signal, considering the complexity of the hysteresis model, which makes the design of the feedback controller difficult. Under the framework of inverse model compensation, a series of hysteresis modeling methods are concerned, such as the Bouc-Wen model [22], Prandtl–Ishlinskii model [23,24], and Preisach [25], and so on. However, the classical hysteresis model can only express the static hysteresis relationship between input and output and cannot accurately establish the rate-dependent hysteresis model of the system. Hence, to perfect the control accuracy in a Piezoelectric actuator, one way is to develop a particularly accurate rate-dependent hysteresis model, such as a neural network [26], improved J-A model [27], and Modular model [28–30] and so on, then use the inverse model for feedforward control. The goal of establishing the inverse model compensation in this article is to connect the static hysteresis inverse model in series in front of the controlled object, to mitigate or even eliminate the effect of static hysteresis nonlinearity in the system, and to realize the conversion of the complex hysteresis nonlinear system into a linear system with certain deviations, which is easy for the design of the controller.

Considering the complexity of the hysteresis nonlinearity of the reluctance motor, which includes displacement-dependent and rate-dependent, multivalued mapping, and memorability, the hysteresis nonlinearity model is hard to establish. Currently, there is no suitable modeling method and control strategy to achieve the control accuracy of reluctance motors. Inspired by [31,32], to suppress the hysteresis nonlinearity of the reluctance motor effectively, the hysteresis model will be divided into two parts: the rate-dependent hysteresis model and the displacement-dependent hysteresis model. In application, following the work of [33–35], we use the Hammerstein model, a widely used rate-dependent modeling method due to its simple structure and convenient controller design. Subsequently, the effect of displacement on the hysteresis model, namely the displacement displacement-dependent hysteresis model, is considered as the disturbance of the Hammerstein model. In practice, the inverse model of the nonlinear part in the Hammerstein model is obtained first, then the inverse model is obtained to eliminate hysteresis nonlinearity and transform the nonlinear system into a linear system with inversion bias and disturbance. It is worth pointing out that the disturbance includes not only the effect of displacement on the hysteresis model but also other disturbances of the system. Last but not least, a reliable controller is designed to achieve high-precision control of the reluctance actuator.

More specifically, in this article, the Hammerstein structure was applied, where the Bouc-Wen model describes the nonlinear characteristics and linear dynamics represents the rate-dependent characteristics of the hysteresis loop, as well as the disturbance term indicating the influence of the displacement on the model and the disturbance caused by modeling error. Thus, the rate-dependent nonlinearity of the reluctance actuator was described. Additionally, considering the system disturbance and model error caused by displacement changes, a new compound control method is designed, which consists of inverse model compensation and the discrete sliding mode controller based on the disturbance observer (DO-DSMC). It is worth noting that the inversion based on the Bouc-Wen model is obtained to compensate for the system's nonlinearity, and the nonlinear system is transformed into a linear system with inversion bias and disturbance. What is more, the sliding mode controller based on the disturbance observer, which is proposed in [36], and was widely used in practical engineering, such as aerospace, industrial control, robot fields, and so on, was adopted due to the advantages of the inherent order reduction properties of the sliding mode variable structure and the invariance of the sliding modes to the parameter uptake and external disturbances of the controlled system, high response speed, strong robustness, and low chattering effect. In this article, taking into account the effect of displacement on the uptake of model parameters, the sliding mode controller based on the

disturbance observer was used to compensate for the unmodeled dynamics, displacement disturbances, and model identification errors in linear systems. The simulation results show that the proposed control strategy makes the system have excellent tracking performance. In general, the specific contributions of this article are as follows:

(1) To identify the parameters of the Hammerstein model of the reluctance actuator, the frequency turning point, which is the frequency inflection point between rate-independent and rate-dependent in the reluctance motor model, was determined for the first time. From the result of identification, we can draw a conclusion that the Hammerstein structure has an excellent effect in modeling rate-dependent hysteresis;

(2) Different from the current reluctance motor research methods, this paper considers the coupling effect of eddy current and displacement on the hysteresis model, which leads to a rate-dependent and displacement-dependent hysteresis effect in the reluctance actuator. Specifically, the Hammerstein model is used to represent the rate-dependent hysteresis, and the displacement-dependent hysteresis effect is regarded as the disturbance of the system;

(3) Compared to existing control methods, the merit of using the novel control strategy lies in that by prespecifying a Hammerstein structure for the reluctance actuator, there are not any simplifications or linearization in dealing with the nonlinear hysteresis, while the controller design is based on the linear rate-dependent part of the reluctance actuator only;

(4) The simulation results show that the proposed control strategy has good robustness to the unmodeled dynamics (the perturbation of displacement to the hysteresis model) and external disturbances of the reluctance motor. In other words, the proposed control strategy has perfect flux tracking ability.

The rest of this paper is organized as follows: According to Hammerstein's structure, the rate-dependent model of the reluctance motor is established in Section 2; it should be indicated that the hysteresis inverse model based on the Bouc-Wen model is obtained. In Section 3, considering the model error and disturbance, the discrete sliding mode control rate based on the disturbance observer is designed. The simulation analysis is given in Section 4. Specifically, it includes the verification of the Hammerstein structure and the feasibility analysis of the proposed control strategy. In addition, inverse model compensation and PI composite strategy, inverse model compensation, and discrete sliding mode composite strategy are carried out. The simulation results show that the proposed control strategy has better performance than the other two control strategies. Afterward, conclusions are addressed in Section 5.

2. Hammerstein Model

This is a rate-dependent model, which can be regarded as the coupling of rate-independent hysteresis model and linear dynamics. In this study, Hammerstein is selected to model the reluctance actuator. More specifically, it is composed of a static nonlinear module and a dynamic linear module, which is depicted in Figure 3. It is worth mentioning that the static module is denoted by the Bouc-Wen model, and the dynamic model is represented by the ARX model.

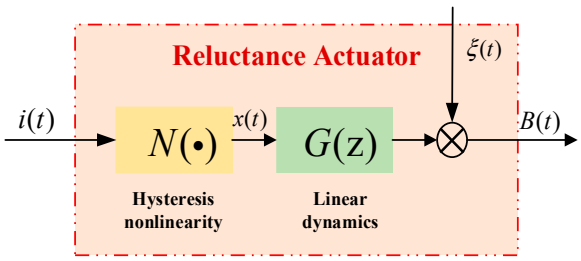

Figure 3. Hammerstein structure.

Where $i(t)$ and are the input and output of the linear reluctance actuator, respectively. Denotes a static nonlinear module, which is described by the Bouc-Wen model. Stand for a linear dynamic module that is described by an autoregressive model with exceptional

input (ARX). It is not only the output of the nonlinear module but also the input signal of the linear module. Furthermore, it indicates a disturbance.

Remark 1. *It is worth noting that various transfer functions such as low-pass filtering model, high pass, band pass, band group, or their composite pattern are used to characterize the linear dynamics of rate-dependent models. However, according to research findings, the ARX model is a time series analysis method whose model parameters gather important information about the system state. An accurate ARX model can deeply and centrally express the operating rules of the system. In addition, it has the advantages of simple structure and easy identification. Therefore, in this article, the ARX model is chosen as the linear dynamics part of the Hammerstein Model.*

2.1. Bouc-Wen Model and Its Inverse Model

The Bouc-Wen model is widely used in hysteresis modeling due to its simple structure, few parameters to be identified, and ease of implementation. Here, the Bouc-Wen model is described in the form of a differential equation, as shown in Equation (1):

$$\begin{cases} \dot{x}(t) = a_0 x(t) + a_1 I(t) + a_2 h(t) \\ \dot{h}(t) = \alpha \dot{I}(t) - \beta |\dot{I}(t)| h(t) - \gamma \dot{I}(t) |h(t) \\ B(t) = x(t) \end{cases} \tag{1}$$

where $x(t)$ represents the state variable of the system, $I(t)$ and $B(t)$ are input current and output flux of the reluctance actuator, respectively. $h(t)$ represents hysteresis, α, β, γ a_0, a_1, a_2 stands for the identification parameters of the Bouc-Wen model. It should be noted that $I(t)$ and $B(t)$ can be directly measured, while $h(t)$ is an intermediate variable that cannot be measured.

The inverse model of the Bouc-Wen model, which can be obtained by a note from (1) that $\dot{x}(t) = a_0 x(t) + a_1 I(t) + a_2 h(t)$, implies:

$$I(t) = \frac{1}{a_1}[\dot{B}_{\mathrm{d}}(t) - a_0 B_{\mathrm{d}}(t) - a_2 \hat{h}(t)] \tag{2}$$

where $B_d(t)$ stands for input trajectory, $I(t)$ represents the input current, a_0, a_1, a_2 is the model parameter, $\hat{h}(t)$ denotes the estimated hysteresis. In addition, it should be indicated that there is no analytic solution to the inverse model, which effectively reduces the mathematical calculation of the controller. What is more, in order to avoid the algebraic ring problem in the algorithm process, the output of the previous time is used instead of the input of the current time $I(t)$.

2.2. ARX Model

The ARX model is a rational transfer function model, which is used to describe the rate-dependent characteristics of the reluctance actuator, and it is defined as Equation (3):

$$A(z^{-1})y(t) = B(z^{-1})w(t) + e(t) \tag{3}$$

where z^{-1} denotes the delay operator, $e(t)$ is an error.

$$\begin{array}{l} A(z^{-1}) = 1 + a_1 z^{-1} + \ldots + a_n z^{-n} \\ B(z^{-1}) = 1 + \mathrm{b}_1 z^{-1} + \ldots + b_m z^{-m} \end{array} \quad c$$

Thus, the ARX model is written as a transfer function:

$$G(z) = \frac{B(z^{-1})}{A(z^{-1})} \tag{4}$$

As such, the rate-dependent hysteresis model of the reluctance actuator based on the Hammerstein structure is established.

3. DO-DSMC Controller Coupled with Hysteresis Compensator

In this paper, a novel control strategy, which consists of inverse model compensation and DO-DSMC, is applied in dealing with the hysteresis effect. Specifically, the control scheme is shown in Figure 4.

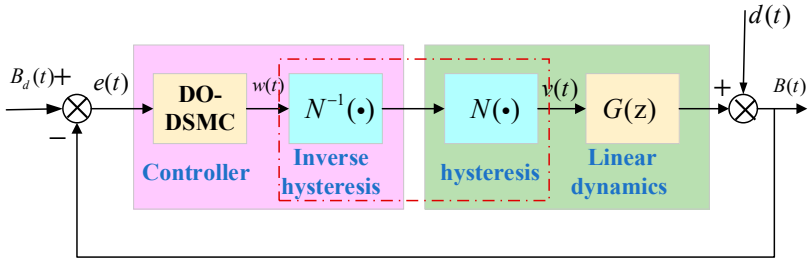

Figure 4. Control scheme.

Here, the inverse model compensator $N^{-1}(\cdot)$ is used to compensate $N(\cdot)$ that is the hysteresis nonlinear part of the reluctance motor system so that $w(t) = v(t)$, and further, the nonlinear system is transformed into a linear system $G(z)$. Thus, to improve the tracking performance of the system, a discrete sliding mode control rate based on the disturbance observer is designed.

3.1. Hysteresis Compensator

As shown in Figure 5, for eliminating the hysteresis nonlinearity of the reluctance actuator, the inverse Bouc-Wen model was obtained in Equation (2), which can directly suppress the hysteresis of the reluctance actuator in different frequencies. Here, when the inverse model and hysteresis model are completely matched, the rate-dependent hysteresis model of the reluctance actuator will be transformed into a linear system, which is represented by $G(z)$.

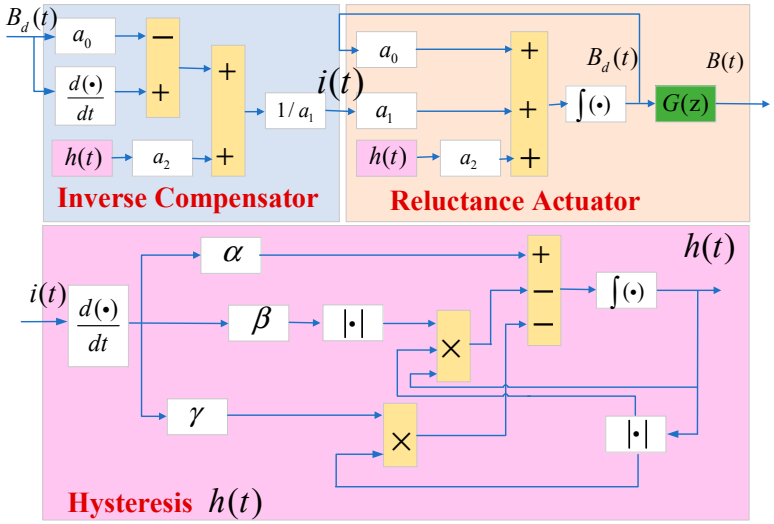

Figure 5. Scheme of the inverse compensation of hysteresis in reluctance actuator.

3.2. Discrete Sliding Mode Control Rate Design Based on Disturbance Observer

In practice, after the inverse model compensation, the nonlinear system is transformed into a linear system with disturbance, namely $G(z)$. In [37], in order to attenuate the

disturbance, the discrete sliding mode control rate design based on the disturbance observer was used. Specifically, the discrete state equation of the system is expressed as Equation (5):

$$x(k+1) = Ax(k) + B[u(k) + d(k)] \tag{5}$$

where $d(k)$ denotes disturbance.

Given input flux signal $x_d(k)$, the tracking error is written as $e(k) = x(k) - x_d(k)$, the sliding surface is expressed as:

$$s(k) = Ce(k) \tag{6}$$

where $C = [c\ 1]^T, c > 0$.

According to Expression (5), the sliding mode control rate with disturbance estimation is designed:

$$u(k) = u_s(k) + u_c(k) \tag{7}$$

What should be explained is that

$$u_s(k) = (C^T B)^{-1}[C^T x_d(k+1) - C^T Ax(k) + qs(k) - \eta \mathrm{sgn}(s(k))] \tag{8}$$

$$u_c(k) = -\hat{d}(k) \tag{9}$$

In (9), $\hat{d}(k)$ is the disturbance observer, which is written as:

$$\hat{d}(k) = \hat{d}(k-1) + (C^T B)^{-1} g[s(k) - qs(k-1) + \eta \mathrm{sgn}(s(k-1))] \tag{10}$$

Assuming $\tilde{d}(k) = d(k) - \hat{d}(k)$, η, q, g is a positive real number.

Combining (5) and (7), Expression (11) is obtained.

$$\begin{aligned} s(k+1) &= C^T e(k+1) = C^T x(k+1) - C^T x_d(k+1) \\ &= C^T(Ax(k) + Bu(k) + Bd(k)) - C^T x_d(k+1) \\ &= C^T Ax(k) + [C^T x_d(k+1) - C^T Ax(k) + qs(k) - \eta \mathrm{sgn}(s(k))] \\ &\quad -C^T B\hat{d}(k) + C^T Bd(k) - C^T x_d(k+1) \\ &= qs(k) - \eta \mathrm{sgn}(s(k)) + C^T B\tilde{d}(k) \end{aligned} \tag{11}$$

According to Equations (10) and (11), we can find

$$\begin{aligned} \tilde{d}(k+1) &= d(k+1) - \tilde{d}(k+1) \\ &= d(k+1) - \hat{d}(k) - (C^T B)^{-1} g[s(k+1) - qs(k) + \eta \mathrm{sgn}(s(k))] \\ &= d(k+1) - d(k) + \tilde{d}(k) - (C^T B)^{-1} g(C^T B)\tilde{d}(k) \\ &= d(k+1) - d(k) - (1-g)\tilde{d}(k) \end{aligned} \tag{12}$$

More specifically, in Appendices A and B, the stability and convergence of the controller are also proved. Specifically, a convergence analysis of disturbance observer is shown in Appendix A and stability analysis was provided in Appendix B.

4. Simulation Analysis

4.1. The Simulated Object

A type of reluctance actuator, as shown in Figure 6, composed of an E-type stator and I-type mover, is designed for this study. It should be emphasized that both the stator and mover are superposed by soft magnetic materials. In practice, when a current is applied to the coil winding on the E-shaped stator, a magnetic field will be generated between E and I, which has a very high magnetic flux density, namely B, thus creating a strong attraction F to the I-shaped mover and driving it to move.

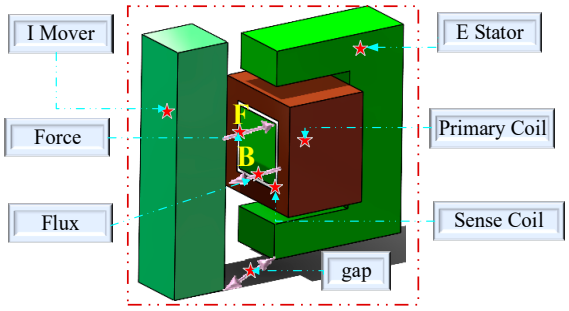

Figure 6. Structure diagram of linear reluctance actuator.

In the COMSOL, the simulation model of the reluctance actuator is established. The main parameters are shown in Table 1.

Table 1. Parameters of reluctance actuator.

Sign	Physical Meaning	Value
A	The cross-sectional area of teeth	960 (mm^2)
N	Coil turns	600
i	current	See paper
g	Air gap	2 mm
Material	Material	CoFe

4.2. Model Identification

According to the Hammerstein structure in Figure 3, which was determined in Chapter 2. Owing to the intermediate variable w(t) not being measurable, the model identification was difficult. In application, rate-dependent characteristics of the linear reluctance actuator, which is caused by the eddy current effect, are in Figure 7.

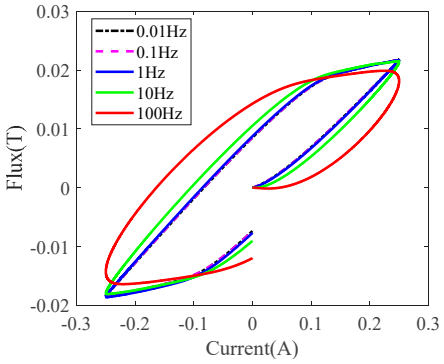

Figure 7. Rate-dependent hysteresis.

Remark 2. *It is worth noting that the hysteresis between the input current and output flux in the reluctance actuator is not only the B-H hysteresis loop of ferromagnetic materials but also closely related to the structure of a linear reluctance motor (such as the flux length). This gives rise to the hysteresis loops shown in Figure 7, which seem larger than is normal for actuators made with soft magnetic steels.*

Theoretically, when the input frequency is low enough, there is no eddy current effect, and it can be considered that it is rate-independent. Thus, at low frequencies, the static nonlinear and the dynamic linear of the Hammerstein model can be separated. Therefore, in this paper, the separation identification method is used to identify the parameters of the Hammerstein structure.

To realize the identification of Hammerstein model parameters, the frequency turning point, which is the frequency inflection point between rate-independent and rate-dependent in the reluctance motor model, was determined by COMSOL first. The result is shown in Figure 8.

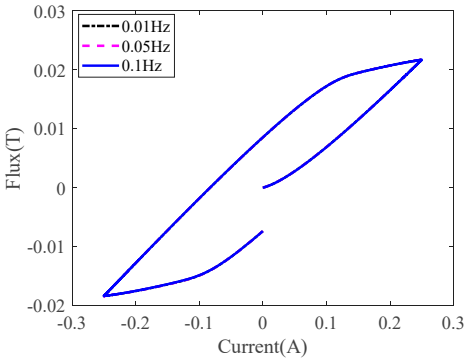

Figure 8. Hysteresis at low frequency.

From Figure 8, we can draw a conclusion that the hysteretic is rate-independent when the reference input signal is lower than 0.1 Hz. Thus, the parameter identification step of the linear reluctance actuator model is shown as follows:

Step 1: A sinusoidal signal i(t) with an excitation frequency not exceeding 0.1 Hz is used to excite the reluctance actuator. Next, the output flux B(t) of the reluctance motor is obtained by the sense coil.

Step 2: From the measurement data (i(t), B(t)), which is obtained by Step 1, the Bouc-Wen model was identified.

Step 3: A sinusoidal scanning signal, with a frequency range of [0 100] Hz, was used to excite the Bouc-Wen model and reluctance motor, respectively. Next, the output data of the Bouc-Wen model was acquired, that is, the internal state variable x(t), as well as the reluctance motor output B(t) were acquired. Eventually, by dataset (x(t), B(t)), the linear part G(z) was identified using the least squares method. The process is shown in Figure 9.

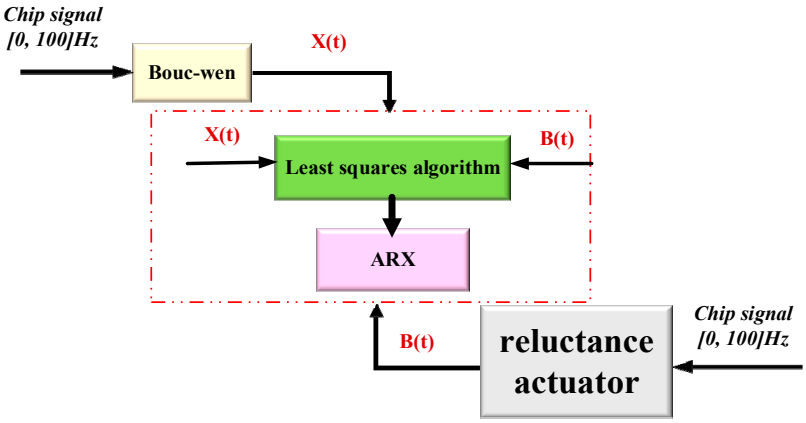

Figure 9. ARX model identification principle.

The accuracy of modeling is expressed by root mean square error (RMSE) and relative error (RE), which are defined as follows:

$$RMSE = \sqrt{\frac{\sum_{i=1}^{N} (\hat{y}(i) - y(i))^2}{N}} \tag{13}$$

$$RE = \sqrt{\frac{\sum_{i=1}^{N} (\hat{y}(i) - y(i))^2}{\sum_{i=1}^{N} (y(i))^2}} \tag{14}$$

Here, $\hat{y}(i)$ denotes the output of the model and $y(i)$ is the output of the reluctance actuator.

4.3. Parameters Identification of Bouc-Wen Model

The TLBO algorithm [37], an intelligent patrol algorithm, is used to identify the parameters of the Bouc-Wen model. The identification principle in the reluctance actuator is shown in Figure 10.

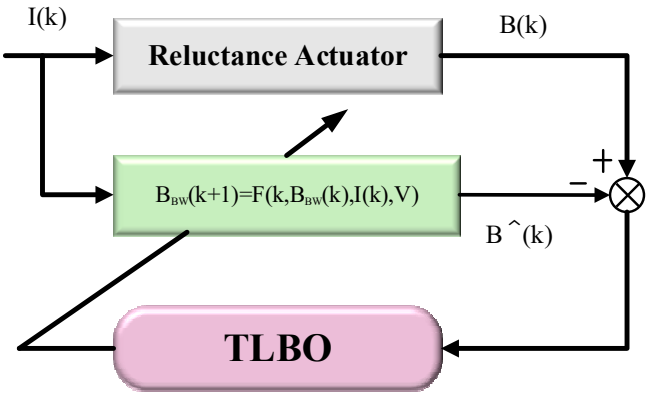

Figure 10. The schematic diagram of Bouc-Wen model identification.

The steps of model identification are as follows:

(1) Data collection: The simulation data, which stands for the reluctance motors model, that is, the hysteresis characteristic between output flux and input current, are obtained by multi-physics simulation software, namely COMSOL. Specifically, the version information is COMSOL Multiphysics 5.5 with MATLAB, and is provided by COMSOL Company in Stockholm, Sweden in 2019.

(2) Model implementation: In Figure 11, the Bouc-Wen model, a classical hysteresis model, was established in MATLAB/Simulink;

(3) Parameter identification: The simulation data are loaded, and then the model parameters are optimized by the TLBO.

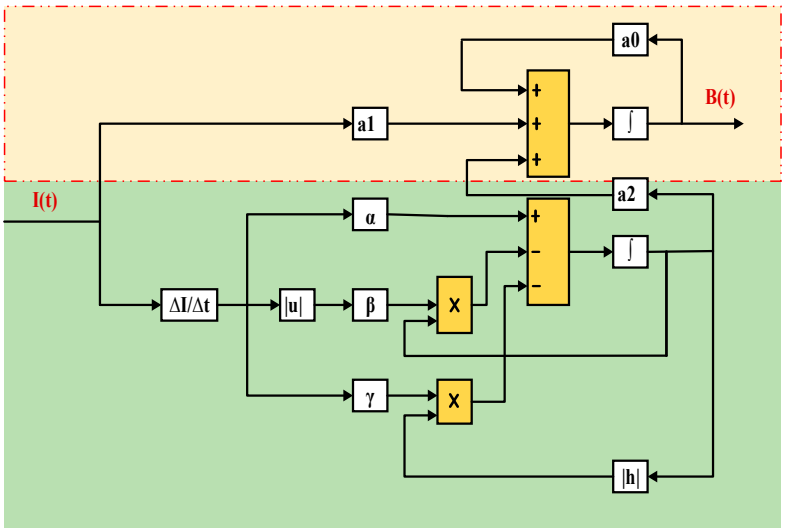

Figure 11. Dynamic simulation model implemented with MATLAB/Simulink.

The identification results are listed in Table 2. Comparing the actual and the fitting data using the estimated Bouc-Wen model, the curves are depicted in Figure 12. We can conclude that the model output matches the actual output well: the RMSE is 4.7926×10^{-6}, and the MSE is 3.3892×10^{-4}.

Table 2. Identified parameters of the classical Bouc-Wen model.

Parameter	Value
a_0	-4170.7
a_1	594.76
a_2	-3294.6
α	0.1203
β	3.6779
γ	1

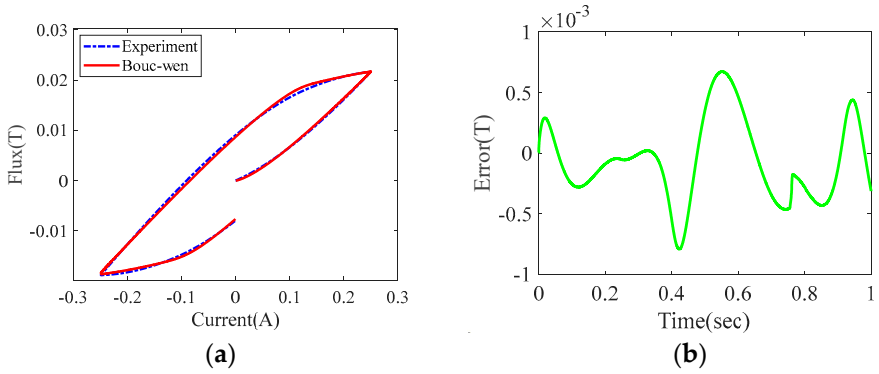

(**a**) (**b**)

Figure 12. Bouc-Wen model identification results: (**a**) Hysteresis loop obtained by experiments and the identified Bouc-Wen model; (**b**) Bouc-Wen model error regarding experimental data.

4.4. Parameters Identification of ARX

Further, to identify the parameters and order of the ARX model, the reluctance actuator system and Bouc-Wen model are excited by the sine sweep signal, respectively. It is added that the change frequency of the sine sweep signal is [0 100] Hz. Then, the dataset $(x(t), B(t))$, which is needed in the process of identifying linear systems, was acquired. As such, by using $x(t)$ as input and $B(t)$ as output and employing the AIC criterion and least square method, respectively, the ARX model is identified as follows:

$$G(z) = \frac{0.1786z - 0.1774}{z^2 - 1.801z + 0.8032} \tag{15}$$

Overall, the rate-dependent hysteresis model based on the Hammerstein structure is established. And it is described in (1), (13), and Table 2.

The identified Hammerstein structure is used to simulate the rate-dependent hysteresis loop, and the simulation effect is shown in Figure 13.

From the figure, we can draw a conclusion that the Hammerstein structure can better simulate the hysteresis loop of the reluctance motor.

Remark 3. *In practice, when the demand for model accuracy is higher, Hammerstein model accuracy, which is not only affected by the composition of each structure, that is, the structural form of nonlinear system and linear dynamics, but also affected by the identification accuracy, can be improved. In application, the nonlinear system of the Hammerstein model is not limited to the Bouc-wen model. Many models that describe the nonlinear relationship of hysteresis, such as the JA and P models, can be applied. Also, in the linear part, the ARX model is not the only choice, and some second-order linear systems that can represent the linear relationship are also used. Meanwhile, the identification method plays an important role in model accuracy. At present, the identification method, which can extract all parameters of the coupled nonlinear static block and the linear dynamic*

block simultaneously, is developed. For the Hammerstein model described previously, however, the more conventional parameter-extraction techniques described below have been found to be adequate. In particular, reluctance motors have rate-independent characteristics at low frequencies; that is, the width of the hysteresis loop does not change with a frequency below 0.1 Hz. In application, the identification method, which is proposed in the paper, is simple and effective.

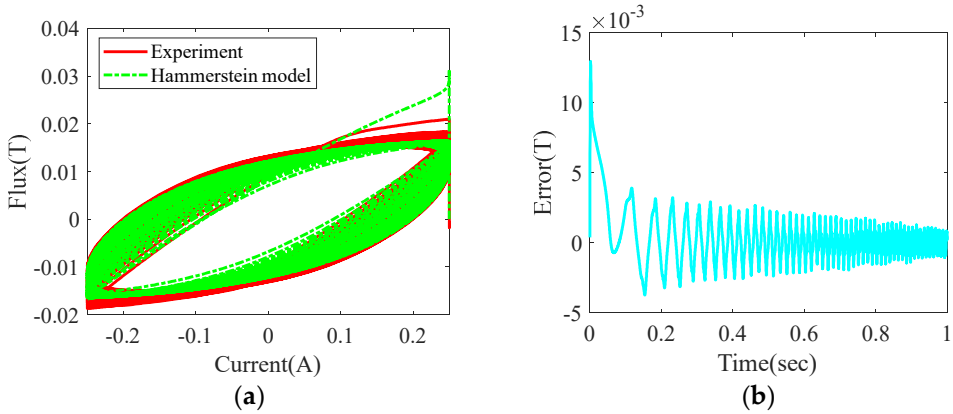

Figure 13. Hammerstein model identification results: (**a**) Hysteresis loop obtained by experiments and the identified Hammerstein model; (**b**) Hammerstein model error with respect to experimental data.

4.5. Model Validation

To verify the accuracy of the Hammerstein model, additional simulation was performed by inputting a group of multiple frequency sine signals, and the sine signals are composed of 0.1/1/10/100 Hz, as shown in Figure 14.

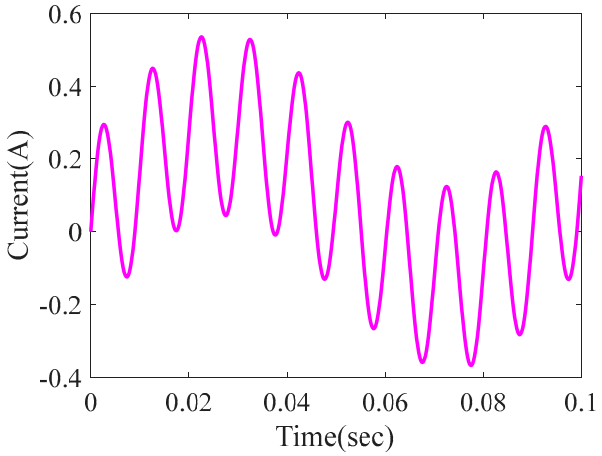

Figure 14. A group of multiple frequency sine signals.

Figure 15 shows the comparison results of the reluctance actuator, Hammerstein model, and Bouc-Wen models. Table 3 gives the accuracy of modeling. From what has been analyzed, we can draw a conclusion that the Hammerstein model has a better matching ability than the Bouc-Wen model.

Specifically, Figure 15a depicts the hysteresis loop obtained by experiments and the identified Hammerstein model. In addition, Figure 15b compares the results between the Bouc-Wen model data and experimental data. In Figure 15c, the red line is the experimental output, the green line indicates the Hammerstein model output, and the blue line represents the Bouc-Wen model output; as seen in Figure 15c, compared with the blue line, the green line is more suitable for the red line, which means that the Hammerstein model fits the reluctance motor model well. Moreover, the fitting error is described in Figure 15d. Obviously, the Hammerstein model has better matching ability than the Bouc-Wen model.

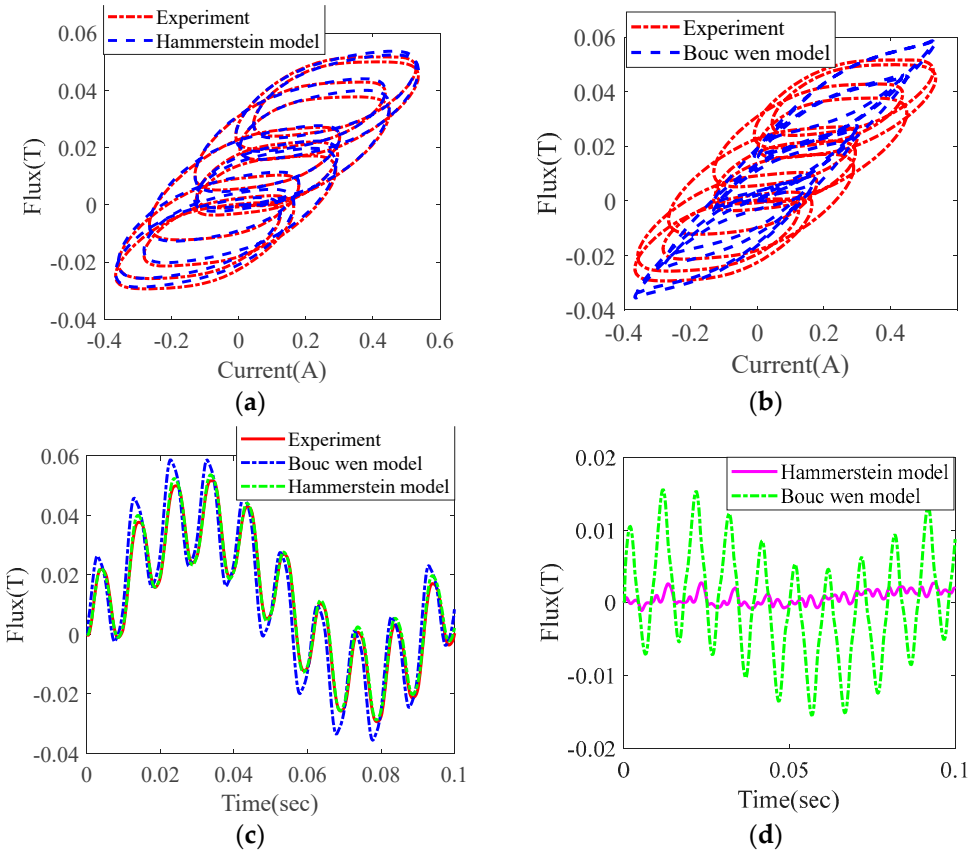

Figure 15. Comparison results of reluctance actuator, Hammerstein model, and Bouc-Wen models. (**a**) Comparison between experiment and Hammerstein model; (**b**) Comparison between experiment and Bouc-Wen model; (**c**) Flux output comparison diagram of the reluctance actuator, Hammerstein model, and Bouc-Wen models; (**d**) The error between Hammerstein model, and Bouc-Wen model and reluctance actuator.

Table 3. The accuracy of modeling.

	Bouc-Wen	**Hammerstein**
RMSE	1.365×10^{-4}	5.299×10^{-5}
RE	0.0097	0.0037

Remark 4. *Many high-precision hysteresis models, including the neural network model, improved operator model, and so on, were proposed in the electromagnetic field. However, it is worth noting that the motive is the pursuit of the appropriate control strategy to reduce the hysteresis effect and heighten the flux tracking accuracy of the reluctance motor in this paper. Therefore, the model accuracy is as important as the design of the controller, whereas in practice, they are contradictory. Specifically, the exact model is proportional to the complexity of its structure; in other words, the higher the accuracy of the model, the more factors are considered in the modeling process and lead to a complex model structure, which further results in a problematic controller design.*

Here, the Hammerstein structure is used to model the reluctance motor due to its structural simplicity and ease of control design controller. Compared with the Bouc-Wen model, the Hammerstein model can better characterize its rate-dependent hysteresis. In the process of comparison, considering the applicability and popularity of the model at the same time, some rate-dependent modeling methods with complex structures, such as the operator model, improved J-A model, and neural network, are popular but not

considered in this paper. Considering the modeling error of the Hammerstein structure, discrete sliding mode control based on the disturbance observer is adopted.

4.6. Simulation

In Figure 16, to suppress the effect of hysteresis, a novel control strategy is applied as follows:

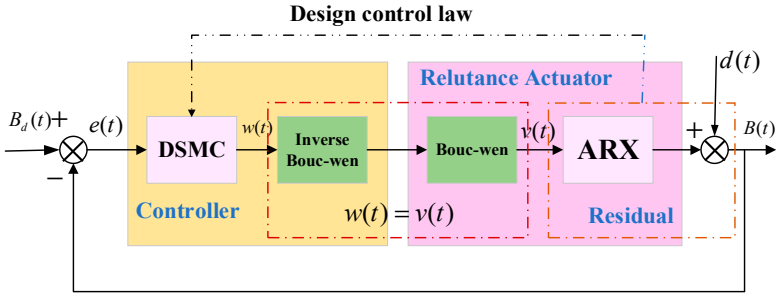

Figure 16. Application diagram of control strategy in reluctance motor.

Actually, in the application of the reluctance actuator, with the desired flux trajectory as an input signal, the DO-DSMC will generate an estimated current, after the inverse hysteresis model and hysteresis model, and driving current. Ideally, the estimated current is equal to the driving current. Under the driving current, the actual flux trajectory is obtained. Hysteresis is the essential characteristic of a reluctance motor, that is, the input current and output flux are nonlinear. If the control strategy is effective, the input flux and output flux will be linear. Therefore, the accuracy of the proposed control strategy can be described by the flux tracking error.

In the simulation, $i = 0.25(\sin(2\pi f_1 t) + \sin(2\pi f_2 t) + \sin(2\pi f_3 t))$ is the inputting signal, and $f_1 = 12Hz; f_2 = 40Hz; f_3 = 80Hz, d(t) = 0.025 \times \sin(2 \times pi \times 5 \times t)$. The control law (7) is adopted, and the sliding mode parameter is adjusted to $c = 9900$, q = 0.79, g = 3.99, η = 0.4531. Figure 17 shows the flux tracking effect of the reluctance actuator.

Specifically, the proposed control strategy, which consists of inverse model compensation and the discrete sliding mode rate based on the disturbance observer, is applied in the reluctance actuator. Figure 17a depicts the input and output trajectories of the reluctance motor. In addition, Figure 17b is the control signal, which implies that the sliding surface is smooth and the chattering effect is suppressed. As seen in Figure 17c, the width of the hysteresis loop has been reduced, which means that the hysteresis effect has been compensated significantly. Moreover, the flux tracking error is described in Figure 17d. Obviously, the novel control method is effective in alleviating hysteresis.

Further, in order to evaluate the effectiveness of the proposed control strategy in this paper, two existing control strategies, which are widely used at present, are also implemented. Namely, the composite control strategy of inverse model compensation and PI control (PI), as well as the compound control strategy of inverse model compensation and discrete sliding mode control (SMC). Figure 18 shows the flux tracking error curves under the three control strategies. Table 4 gives the experimental result of flux tracking control in different control strategies.

The simulation results are shown in Figure 18. Figure 18a describes the input trajectory and the output trajectory under the three controllers. Figure 18b is the tracking error under the three controllers, which implies the tracking performance in different controllers. Where the red line, green line, and purple line are the tracking error under PI, DSMC, and DO-DSMC controller, respectively, we can see that the purple tracking error is the minimum; that is, the tracking performance of DO-DSMC is higher than DSMC and superior to PI controller. In practice, compared with the PI controller, DSMC has better disturbance rejection ability, whereas, when the disturbance is large, the system will be unstable, and the disturbance has an influence on tracking error. From Figure 18b, the green curve described the phenomenon, that is, after the green curve reaches stability, the

overall error is also affected by disturbance. DO-DSMC, which is more stable than DSMC due to the introduction of a disturbance observer, is shown in purple in Figure 18b, where the disturbance observer compensates for the disturbances in the system, which improves the convergence and stability of the system.

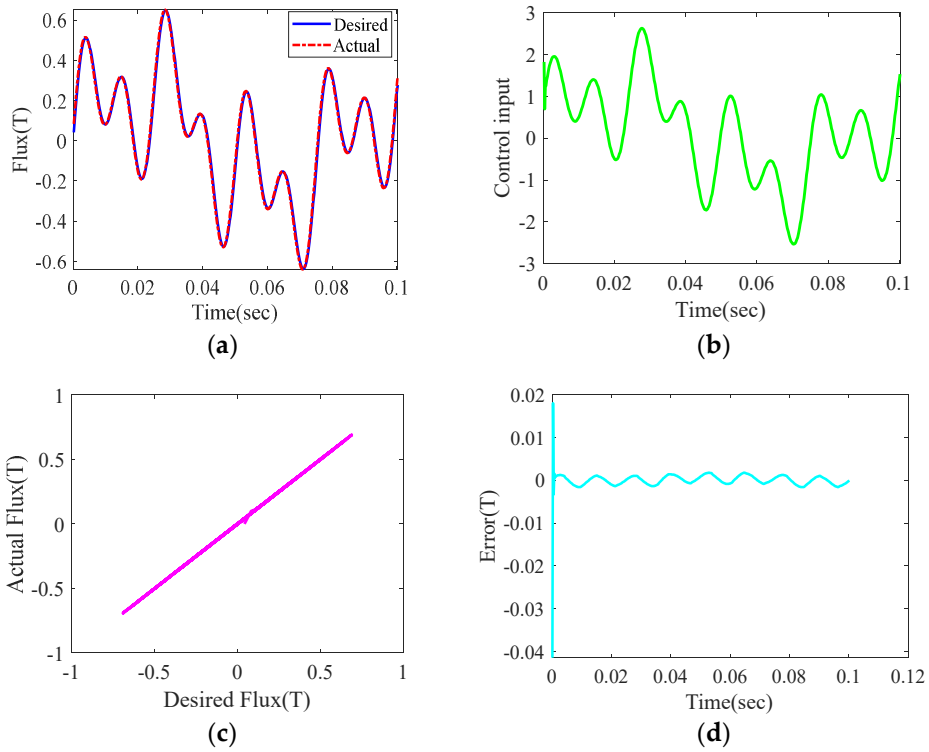

Figure 17. Multi-frequency sinusoidal trajectory tracking results. (**a**) Desired and actual flux trajectories; (**b**) Input control of reluctance motor; (**c**) Actual versus desired flux; (**d**) Control effort of the controller.

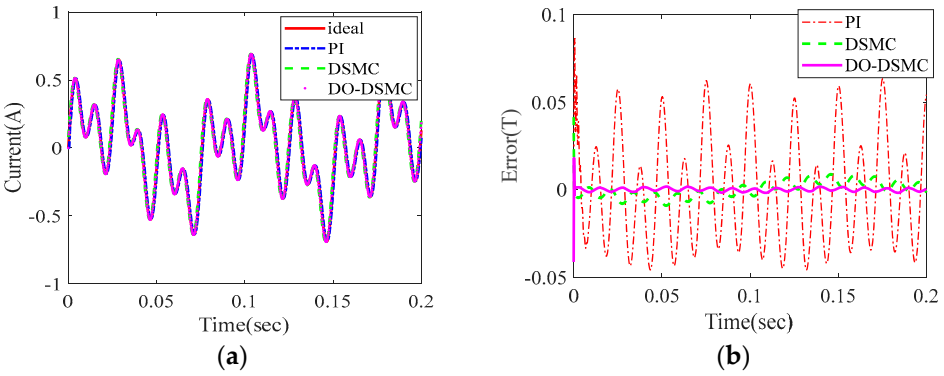

Figure 18. The flux tracking error curves under the three control strategies. (**a**) Desired and actual flux trajectories; (**b**) Control effort of the controller.

Table 4. The control effort of flux tracking control in different control strategies.

	Var	MSE	RE
PI	9.5549×10^{-4}	6.1810×10^{-4}	0.0309
DSMC	1.9755×10^{-5}	8.9836×10^{-5}	0.0045
DO-DSMC	1.6813×10^{-6}	2.5928×10^{-5}	0.0013

Further, in order to evaluate the control performance of the three controllers, some indexes, including VAR, MSE, and RE, were introduced, reflecting the change degree of

tracking error data, namely, the stability of the system. Where VAR is variance, MSE denotes the mean square error, and RE stands for relative error. The analysis results are shown in Table 4 and Figure 19. Figure 19 depicts the index contribution of three controllers under each index, where the abscissa and ordinate are the indexes and the proportion of each controller, respectively. From what has been mentioned, we can draw a conclusion that, under any index, the proportion of the PI controller is higher than DSMC and DO-DSMC, which means that the stability of discrete sliding film controller based on the disturbance observer is more excellent than the other two controllers.

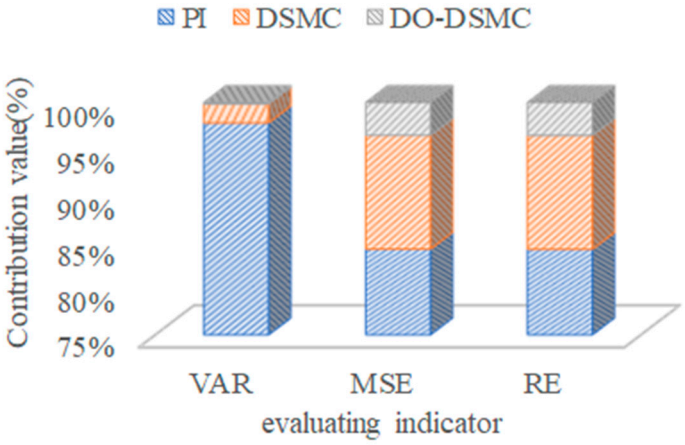

Figure 19. Tracking the performance of three controllers.

Hence, from the simulation results, which are shown in Figures 18 and 19 and Table 4, we can see that the new control strategy is superior to the PI controller combined with inverse compensator and even DSMC combined with inverse compensator. Thus, we can draw a conclusion that the novel control strategy, namely the composite control strategy consisting of inverse model compensation and DO-DSMC, is effective in reducing hysteresis nonlinearity.

5. Conclusions and Discussion

In this paper, the Hammerstein structure is used to describe the rate-dependent hysteresis characteristics of linear reluctance actuators. From the result of identification, we can draw a conclusion that Hammerstein's structure has an excellent effect in modeling the rate-dependent hysteresis. Meanwhile, a new control strategy that combines inverse model compensation and the discrete sliding mode control based on the disturbance observer was proposed, which can effectively suppress the hysteresis effect. To evaluate the effectiveness of the proposed control strategy, two existing control strategies, which are widely used at present, are also implemented. The simulation results show that it is superior to the PI controller combined with inverse compensator and even DSMC combined with inverse compensator, and confirm the effectiveness of the novel control method in alleviating hysteresis. Next, applying the algorithm in this article to the reluctance motor and achieving high-precision flux tracking control of the reluctance motor will be the research focus of our future work.

Author Contributions: Conceptualization, Y.L. and Q.M.; methodology, Q.M. and Y.D.; software, Q.M.; validation, Y.L. and Y.D.; formal analysis, Q.M.; investigation, Y.D.; resources, Y.L.; writing—original draft preparation, Q.M.; writing—review and editing, Y.L. and Y.D.; supervision, Y.L. All authors have read and agreed to the published version of the manuscript.

Funding: This work is supported by the National Natural Science Foundation of China (52075132 and 52105546) and the Opening Foundation of State Key Lab of Digital Manufacturing Equipment & Technology, China DMETKF2020024.

Institutional Review Board Statement: Not applicable.

Informed Consent Statement: Not applicable.

Data Availability Statement: No new data were created.

Conflicts of Interest: The authors declare no conflict of interest.

Appendix A. A Convergence Analysis of Disturbance Observer

Theorem A1 [37]. *For the disturbance observer (10), there is a positive constant m, if* $|d(k+1) - d(k)| < m$, *then there is* k_0, *when* $k > k_0$, *we can draw a conclusion that* $\widetilde{d}(k) < m/g$, *where,* $0 < g < 1$.

Proving: First, decompose $\widetilde{d}(k)$ into:

$$\widetilde{d}(k) = \widetilde{d_1}(k) + \widetilde{d_2}(k) \tag{A1}$$

Setting $\widetilde{d_1}(0) = 0$, and $\widetilde{d_2}(0) = \widetilde{d_1}(0)$, from the expression (A1), we can see that

$$\widetilde{d}(k+1) = \widetilde{d_1}(k+1) + \widetilde{d_2}(k+1) \tag{A2}$$

According to Equation (12), it can be obtained

$$\widetilde{d}(k+1) = (1-g)\widetilde{d_2}(k) \tag{A3}$$

Next, to prove $\widetilde{d_1}(k) < m/g$, induction is applied and the details are as follows,

(1) When $k = 0$, $\widetilde{d_1}(0) = 0 < m/g$

(2) Assuming $\left|\widetilde{d_1}(k)\right| < m/g$, and combining the Equation (A2) and $0 < g < 1$, when $k+1$, we can see that,

$$\begin{aligned} \left|\widetilde{d_1}(k+1)\right| &\leq (1-g)\left|\widetilde{d_1}(k)\right| + |d(k+1) - d(k)| \\ &< (1-g)\tfrac{m}{g} + m = \tfrac{m}{g} \end{aligned} \tag{A4}$$

From what has been mentioned, we can draw a conclusion that

$$\left|\widetilde{d_1}(k)\right| < \frac{m}{g},\ k \geq 0 \tag{A5}$$

By considering Equation (A3) and $0 < 1 - g < 1$, we obtain

$$\widetilde{d_2}(k+1) = (1-g)\widetilde{d_2}(k) \leq (1-g)\left|\widetilde{d_2}(k)\right| < \widetilde{d_2}(k) \tag{A6}$$

Thus, it is obvious that $\widetilde{d_2}(k)$ is a decreasing function, that is, there is k_0', when $k > k_0'$, $\widetilde{d_2}(k)$ can be any small.

Eventually, we can verify a result as shown in Equation (A7). Specifically, there is k_0 and when $k > k_0$, we obtain

$$\left|\widetilde{d}(k)\right| = \left|\widetilde{d_1}(k) + \widetilde{d_2}(k)\right| \leq \left|\widetilde{d_1}(k)\right| + \left|\widetilde{d_2}(k)\right| < \frac{m}{g} \tag{A7}$$

Appendix B. Stability Analysis

Theorem A2 [37]. *For the disturbance observer (10), the stability conditions of the closed loop system are as follows:*

(1) $0 < q < 1, 0 < g < 1$

(2) There is a positive constant m, $|d(k+1) - d(k)| < m$
(3) $0 < C^T B < \eta$

The detailed proof is as follows:
Set $v(k) = C^T B \frac{m}{g} \hat{d}(k)$, and obtain

$$|v(k)| < C^T B \frac{m}{g} < \eta \tag{A8}$$

That is,

$$-C^T B \frac{m}{g} < v(k) < C^T B \frac{m}{g} \tag{A9}$$

Equation (12) can be written as

$$s(k+1) = qs(k) - \eta \mathrm{sgn}(s(k)) + v(k) \tag{A10}$$

Then, we will analyze the stability of the system from the following four aspects:
Case 1: $s(k) \geq C^T B \frac{m}{g} + \eta > 0$

$$s(k+1) - s(k) = (q-1)s(k) - \eta + v(k) < 0 \tag{A11}$$

$$\begin{aligned} s(k+1) + s(k) &= (q+1)s(k) - \eta + v(k) \\ &\geq (q+1)(C^T B \tfrac{m}{g} + \eta) - \eta + v(k) \\ &= q(C^T B \tfrac{m}{g} + \eta) + C^T B \tfrac{m}{g} + v(k) > 0 \end{aligned} \tag{A12}$$

Obviously,

$$s(k+1)^2 < s(k)^2 \tag{A13}$$

Case 2: $s(k) \leq -C^T B \frac{m}{g} - \eta < 0$

$$s(k+1) - s(k) = (q-1)s(k) + \eta + v(k) > 0 \tag{A14}$$

$$\begin{aligned} s(k+1) + s(k) &= (q+1)s(k) + \eta + v(k) \\ &< s(k) + \eta + v(k) \\ &\leq -C^T B \tfrac{m}{g} - \eta + \eta + v(k) \\ &= C^T B \tfrac{m}{g} + v(k) < 0 \end{aligned} \tag{A15}$$

Then,

$$s(k+1)^2 < s(k)^2 \tag{A16}$$

Case 3: $0 < s(k) < C^T B \frac{m}{g} + \eta$

$$\begin{aligned} s(k+1) &= qs(k) - \eta + v(k) < q(C^T B \tfrac{m}{g} + \eta) - \eta + v(k) \\ &< q(C^T B \tfrac{m}{g} + \eta) < C^T B \tfrac{m}{g} + \eta \end{aligned} \tag{A17}$$

Then,

$$|s(k+1)| < C^T B \frac{m}{g} + \eta \tag{A18}$$

Case 4: $-C^T B \frac{m}{g} - \eta < s(k) < 0$

$$\begin{aligned} s(k+1) &= qs(k) + \eta + v(k) > s(k) + \eta + v(k) \\ &> -C^T B \tfrac{m}{g} - \eta + \eta + v(k) > -C^T B \tfrac{m}{g} - \eta \end{aligned} \tag{A19}$$

$$s(k+1) = qs(k) + \eta + v(k) < \eta + v(k) < C^T B \frac{m}{g} + \eta \tag{A20}$$

Then,

$$|s(k+1)| < C^T B\frac{m}{g} + \eta \tag{A21}$$

From what has been mentioned, we can draw a conclusion as follows,

(1) When $|s(k)| \geq C^T B\frac{m}{g} + \eta$, that is $s(k+1)^2 < s(k)^2$

(2) When $|s(k)| < C^T B\frac{m}{g} + \eta$, that is $|s(k+1)| < C^T B\frac{m}{g} + \eta$

Since disturbance $d(t)$ is continuous, as long as the sampling time is small enough, $|d(k+1) - d(k)| < m$ can be guaranteed. Where, in order to ensure $\frac{m}{g} \ll 1$, m should be a very small positive real number. What is more, because of $C^T B\frac{m}{g} < \eta$, as long as η is a very small positive real number, then $C^T B\frac{m}{g} + \eta \leq 1$ was obtained; ultimately, convergence of $s(k+1)$ is guaranteed.

References

1. Song, F.Z.; Liu, Y.; Jin, W.; Tan, J.B.; He, W. Data-Driven Feedforward Learning with Force Ripple Compensation for Wafer Stages: A Variable-Gain Robust Approach. *IEEE Trans. Neural Netw. Learn. Syst.* **2022**, *33*, 1594–1608. [CrossRef] [PubMed]
2. Li, L.; Liu, Y.; Li, L.Y.; Tan, J.B. Kalman-Filtering-Based Iterative Feedforward Tuning in Presence of Stochastic Noise: With Application to a Wafer Stage. *IEEE Trans. Ind. Inform.* **2019**, *15*, 5816–5826. [CrossRef]
3. Kuang, Z.; Sun, L.T.; Gao, H.J.; Tomizuka, M. Practical Fractional-Order Variable-Gain Supertwisting Control with Application to Wafer Stages of Photolithography Systems. *IEEE-ASME Trans. Mechatron.* **2022**, *27*, 214–224. [CrossRef]
4. Boeren, F.; Lanzon, A.; Oomen, T. Iterative Identification and Control Using Non-normalized Coprime Factors with Application in Wafer Stage Motion Control. *IEEE Trans. Control Syst. Technol.* **2020**, *28*, 413–424. [CrossRef]
5. Song, F.Z.; Liu, Y.; Xu, J.X.; Yang, X.F.; He, P.; Yang, Z.L. Itrative learning identification and compensation of space-periodic disturbance in PMLSM systems with time delay. *IEEE Trans. Ind. Electron.* **2018**, *65*, 7579–7589. [CrossRef]
6. Liu, Y.; Li, L.; Yang, X.F.; Tan, J.B. Enhanced kalman-filtering iterative learning control with application to a wafer scanner. *Inf. Sci.* **2020**, *541*, 152–165. [CrossRef]
7. Al Saaideh, M.; Alatawneh, N.; Al Janaideh, M. Design parameters of a reluctance actuation system for stable operation conditions with applications of high-precision motions in lithography machines. *IET Electr. Power Appl.* **2022**, *16*, 68–85. [CrossRef]
8. Ito, S.; Cigarini, F.; Schitter, G. Flux-Controlled Hybrid Reluctance Actuator for High-Precision Scanning Motion. *IEEE Trans. Ind. Electron.* **2020**, *67*, 9593–9600. [CrossRef]
9. Katalenic, A.; Butler, H.; van den Bosch, P.P.J. High-Precision Force Control of Short-Stroke Reluctance Actuators with an Air Gap Observer. *IEEE-ASME Trans. Mechatron.* **2016**, *5*, 2431–2439. [CrossRef]
10. MacKenzie, I.; Trumper, D.L. Real-Time Hysteresis Modeling of a Reluctance Actuator Using a Sheared-Hysteresis-Model Observer. *IEEE-ASME Trans. Mechatron.* **2016**, *21*, 4–16. [CrossRef]
11. Katalenic, A.; de Boeij, J.; Butler, H.; van den Bosch, P.P.J. Linearization of a current-driven reluctance actuator with hysteresis compensation. *Mechatronics* **2013**, *23*, 163–171. [CrossRef]
12. Ramirez-Laboreo, E.; Roes, M.G.L.; Sagues, C. Hybrid Dynamical Model for Reluctance Actuators Including Saturation, Hysteresis, and Eddy Currents. *IEEE-ASME Trans. Mechatron.* **2019**, *3*, 1396–1406. [CrossRef]
13. Xu, Y.L.; Li, X.P.; Yang, X.F.; Yang, Z.L.; Wu, L.W.; Chen, Q.S. A two-stage model for rate-dependent inverse hysteresis in reluctance actuators. *Mech. Syst. Signal Process.* **2020**, *135*, 106427. [CrossRef]
14. Ahmed, K.; Yan, P.; Li, S. Duhem Model-Based Hysteresis Identification in Piezo-Actuated Nano-Stage Using Modified Particle Swarm Optimization. *Micromachines* **2021**, *3*, 315. [CrossRef]
15. Kim, H.G.; Kim, J.N.; Na, T.W.; Park, K.C.; Oh, I.K. Motion Control of Piezoelectric Tripod Platform via Feedforward Hysteresis Compensation. *Adv. Mater. Technol.* **2019**, *12*, 1800298. [CrossRef]
16. Li, P.Z.; Zhang, D.F.; Hu, J.Y.; Lennox, B.; Arvin, F. Hysteresis Modelling and Feedforward Control of Piezoelectric Actuator Based on Simplified Interval Type-2 Fuzzy System. *Sensors* **2020**, *9*, 2587. [CrossRef] [PubMed]
17. Jian, Y.J.; Huang, D.Q.; Liu, J.B.; Min, D. High-Precision Tracking of Piezoelectric Actuator Using Iterative Learning Control and Direct Inverse Compensation of Hysteresis. *IEEE Trans. Ind. Electron.* **2019**, *1*, 368–377. [CrossRef]
18. Yang, L.; Ding, B.X.; Liao, W.H.; Li, Y.M. Identification of Preisach Model Parameters Based on an Improved Particle Swarm Optimization Method for Piezoelectric Actuators in Micro-Manufacturing Stages. *Micromachines* **2022**, *5*, 698. [CrossRef]
19. Nie, L.L.; Luo, Y.L.; Gao, W.; Zhou, M.L. Rate-dependent asymmetric hysteresis modeling and robust adaptive trajectory tracking for piezoelectric micropositioning stages. *Nonlinear Dyn.* **2022**, *3*, 2023–2043. [CrossRef]
20. Main, J.A.; Garcia, E.; Newton, D.V. Precision position control of piezoelectric actuators using charge feedback. *J. Guid. Control Dyn.* **1995**, *5*, 1068–1073. [CrossRef]
21. Li, Y.; Xu, Q. Adaptive sliding mode control with perturbation estimation and pid sliding surface for motion tracking of a piezo-driven micromanipulator. Control Systems Technology. *IEEE Trans. Control Syst. Technol.* **2010**, *18*, 798–810. [CrossRef]

22. Li, C.X.; Li, L.L.; Gu, G.Y.; Zhu, L.M. Modeling of Rate-Dependent Hysteresis in Piezoelectric Actuators Using a Hammerstein-Like Structure with a Modified Bouc-Wen Model. *Lect. Notes Artif. Intell.* **2016**, *9834*, 672–684.
23. Zhang, Z.; Yang, X.Y.; Pang, W.T.; Zhou, K.M. Hammerstein system identification in the presence of threshold-discrete Prandtl-Ishlinskii Operator and its application in piezoelectric actuator. In Proceedings of the 36th Chinese Control Conference (CCC 2017), Dalian, China, 26–28 July 2017; pp. 2204–2209.
24. Zhao, Y.H.; Meng, G.; Zhang, W.M. Characterization and modeling of viscoelastic hysteresis in a dielectric elastomer actuator. *Smart Mater. Struct.* **2020**, *5*, 055019. [CrossRef]
25. Zhang, H.T.; Hu, B.; Li, L.L.; Chen, Z.Y.; Wu, D.R.; Xu, B.W.; Huang, X.; Gu, G.Y.; Yuan, Y. Distributed Hammerstein Modeling for Cross-Coupling Effect of Multiaxis Piezoelectric Micropositioning Stages. *IEEE-ASME Trans. Mechatron.* **2019**, *6*, 2794–2804. [CrossRef]
26. Ahmed, K.; Yan, P. Modeling and Identification of Rate Dependent Hysteresis in Piezoelectric Actuated Nano-Stage: A Gray Box Neural Network Based Approach. *IEEE Access* **2021**, *9*, 65440–65448. [CrossRef]
27. Chen, L.; Zhang, Z.Y.; Ben, T.; Zha, H.Y. Dynamic Magnetic Hysteresis Modeling Based on Improved Parametric Magneto-Dynamic Model. *IEEE Trans. Appl. Supercond.* **2022**, *6*, 0600605. [CrossRef]
28. Wills, A.; Ninness, B. Generalised Hammerstein-Wiener system estimation and a benchmark application. *Control Eng. Pract.* **2012**, *11*, 1097–1108. [CrossRef]
29. Qi, C.K.; Gao, F.; Li, H.X.; Li, S.Y.; Zhao, X.C.; Dong, Y. An incremental Hammerstein-like modeling approach for the decoupled creep, vibration and hysteresis dynamics of piezoelectric actuator. *Nonlinear Dyn.* **2015**, *4*, 2097–2118. [CrossRef]
30. Napole, C.; Barambones, O.; Calvo, I.; Derbeli, M.; Silaa, M.Y.; Velasco, J. Advances in Tracking Control for Piezoelectric Actuators Using Fuzzy Logic and Hammerstein-Wiener Compensation. *Mathematics* **2020**, *11*, 2071. [CrossRef]
31. Al Janaideh, M.; Rakotondrabe, M. Precision motion control of a piezoelectric cantilever positioning system with rate-dependent hysteresis nonlinearities. *Nonlinear Dyn.* **2021**, *4*, 3385–3405. [CrossRef]
32. Zhou, J.L.; Dong, L.H.; Yang, W.D. Hysteresis Compensation for a Piezoelectric Actuator of Active Helicopter Rotor Using Compound Control. *Micromachines* **2022**, *11*, 1298. [CrossRef] [PubMed]
33. Gan, J.Q.; Zhang, X.M. Nonlinear Hysteresis Modeling of Piezoelectric Actuators Using a Generalized Bouc-Wen Model. *Micromachines* **2019**, *3*, 183. [CrossRef]
34. Liu, J.B.; Zou, Q.Z. On superposition of Hammerstein systems: Application to simultaneous hysteresis-dynamics compensation. *Int. J. Robust Nonlinear Control* **2018**, *14*, 4075–4092. [CrossRef]
35. Miguel, G.; Niklas, E.; Håkan, H. ARX modeling of unstable linear systems. *Automatica* **2017**, *75*, 167–171.
36. Eun, Y.; Kim, J.H.; Kim, K.; Cho, D.I. Discrete-time variable structure controller with a decoupled disturbance compensator and its application to a CNC servomechanism. *IEEE Trans. Control Syst. Technol.* **1999**, *4*, 414–423.
37. Miao, Q.; Liu, Y.; Tan, J.B. Precision Flux Control of Linear Reluctance Actuator Using the Integral Sliding Mode Method. *Front. Energy Res.* **2022**, *10*, 949782. [CrossRef]

Disclaimer/Publisher's Note: The statements, opinions and data contained in all publications are solely those of the individual author(s) and contributor(s) and not of MDPI and/or the editor(s). MDPI and/or the editor(s) disclaim responsibility for any injury to people or property resulting from any ideas, methods, instructions or products referred to in the content.